

Quantum simulator for the Schwinger effect with atoms in an optical lattice

Nikodem Szpak* and Ralf Schützhold†

Fakultät für Physik, Universität Duisburg-Essen, Duisburg, Germany

(Dated: March 21, 2019)

Ultra-cold atoms in specifically designed optical lattices can be used to mimic the many-particle Hamiltonian of QED describing electrons and positrons in an external electric field. This facilitates the experimental simulation of (so far unobserved) fundamental quantum phenomena such as the Schwinger effect, i.e., the electron-positron pair creation out of the vacuum by a strong electric field.

Introduction There are several fundamental predictions of relativistic quantum field theory which have so far eluded a direct experimental verification. One prominent example is the Schwinger [1] effect (historically more correct would be the name Sauter-Schwinger effect, see [2] and [3]), i.e., the creation of electron/positron-pairs out of the vacuum by a strong electric field. For a constant electric field E , the leading order e^+e^- pair creation probability scales as [1–3]

$$P_{e^+e^-} \sim \exp \left\{ -\pi \frac{c^3}{\hbar} \frac{M^2}{qE} \right\} = \exp \left\{ -\pi \frac{E_S}{E} \right\}, \quad (1)$$

where $E_S = M^2 c^3 / (\hbar q)$ is the critical field strength determined by the charge q and the mass M of an electron (or positron). The above expression (1) for $P_{e^+e^-}$ does not permit a Taylor expansion in q , i.e., it is inherently non-perturbative and cannot be represented by any finite set of Feynman diagrams.

Unfortunately, our theoretical understanding of this non-perturbative QED effect is still very incomplete. Apart from the constant field case, only very simple field configurations where the electric field either depends on time $E(t)$ or on one spatial coordinate such as $E(x)$ are fully solved. For example, recently it has been found that the occurrence of two different frequency scales in a time-dependent field $E(t)$ can induce drastic changes in the (momentum dependent) pair creation probability [4–6]. Moreover, the impact of interactions between the electron and the positron of the created pair, as well as between them and other electrons/positrons is not understood. This ignorance is unsatisfactory not only from a theory point of view but also in view of planned experiments (see, e.g., [7]) which envisage field strengths not too far below the critical field strength E_S and thus could be able to probe this effect experimentally.

These considerations motivate the investigation of the Schwinger effect via a different line of approach. By suitably designing a laboratory system, we could reproduce the quantum many-particle Hamiltonian of QED describing electrons and positrons in an electric field and thereby obtain a quantum simulator for the Schwinger effect. This would facilitate the investigation of space-time dependent electric fields such as $E(t, x)$ and could also provide some insight into the role of interactions. It should be noted here that our proposal goes beyond the

simulation of the (classical) Dirac equation, see, e.g. [9–17], as not only the relativistic energy spectrum but also the *canonical anticommutation relations* for the particle/hole creation and annihilation operators are essential to assure the correct features of the many-particle system. It is somewhat related to the recent observation of the Klein paradox in graphene [18, 19], but in this case, there was no mass gap – which is crucial for studying the non-perturbative Schwinger effect, cf. Eq. (1).

The model We consider the Dirac equation [8] describing electrons/positrons propagating in an electromagnetic vector potential A_μ which are described by the spinor wave-function Ψ ($\hbar = c = 1$)

$$\gamma^\mu (i\partial_\mu - qA_\mu)\Psi - M\Psi = 0. \quad (2)$$

For simplicity, we consider 1+1 dimensions ($\mu = 0, 1$) where the Dirac matrices γ^μ satisfying the Clifford algebra $\{\gamma^\mu, \gamma^\nu\} = 2\eta^{\mu\nu}$ can be represented by Pauli matrices $\gamma^0 = \sigma_3 = \sigma_z$ and $\gamma^1 = -i\sigma_1 = -i\sigma_x$. Furthermore, we can choose the gauge $qA_0 = \Phi$ and $A_1 = 0$ (because in one spatial dimension, there is no magnetic field). As a result, the Dirac equation simplifies to

$$i\partial_t\Psi(t, x) = (-i\sigma_2\partial_x + M\sigma_3 + \Phi)\Psi(t, x). \quad (3)$$

In one spatial dimension, there is also no spin, hence the wave function has only two components $\Psi = (\Psi^1, \Psi^2)$. The Hamiltonian for the classical Dirac field reads then

$$H = \int dx \Psi^\dagger (-i\sigma_2\partial_x + M\sigma_3 + \Phi)\Psi. \quad (4)$$

As the next step, we discretize the space dimension and introduce a regular grid (lattice) $x_n = na$ with a positive grid (lattice) constant a and integers $n \in \mathbb{Z}$. The discretization of the wave function $\Psi_n(t) := \sqrt{a}\Psi(t, x_n)$, defined now at the grid points x_n , gives rise to a discretized derivative $\sqrt{a}\partial_x\Psi(t, x_n) \rightarrow [\Psi_{n+1}(t) - \Psi_{n-1}(t)]/(2a)$. Finally, replacing the x -integral by a sum, we obtain

$$H \rightarrow \sum_n \Psi_n^\dagger \left[-\frac{i\sigma_2}{2a}(\Psi_{n+1} - \Psi_{n-1}) + M\sigma_3\Psi_n + \Phi\Psi_n \right]. \quad (5)$$

In order to obtain the quantum many-body Hamiltonian, we quantize the discretized Dirac field operators via the fermionic anti-commutation relations

$$\{\hat{\Psi}_n^\alpha(t), \hat{\Psi}_m^\beta(t)\} = 0, \quad \{\hat{\Psi}_n^\alpha(t), [\hat{\Psi}_m^\beta(t)]^\dagger\} = \delta_{n,m}. \quad (6)$$

Using $\hat{\Psi}_n = (\hat{a}_n, \hat{b}_n)$, i.e., $\hat{\Psi}_n^1 = \hat{a}_n$ and $\hat{\Psi}_n^2 = \hat{b}_n$, the discretized many-particle Hamiltonian reads

$$\hat{H} = \frac{1}{2a} \sum_n \left[\hat{b}_{n+1}^\dagger \hat{a}_n - \hat{b}_n^\dagger \hat{a}_{n+1} + \text{h.c.} \right] + \sum_n \left[(\Phi_n + M) \hat{a}_n^\dagger \hat{a}_n + (\Phi_n - M) \hat{b}_n^\dagger \hat{b}_n \right]. \quad (7)$$

The first term describes jumping between the neighboring grid points while the remaining two terms can be treated as a combination of external potentials. Due to the specific form of the jumping, the lattice splits into two disconnected sub-lattices: (A) containing \hat{a}_{2n} and \hat{b}_{2n+1} and (B) containing \hat{a}_{2n+1} and \hat{b}_{2n} with integers n . Since the two sub-lattices behave basically in the same way, it is sufficient to consider only one of them, say A. With a re-definition of the local phases via $\hat{a}_{2n} \rightarrow (-1)^n \hat{a}_{2n}$ and $\hat{b}_{2n+1} \rightarrow (-1)^{n+1} \hat{b}_{2n+1}$, we obtain (for sub-lattice A)

$$\hat{H} = -\frac{1}{2a} \sum_n \left[\hat{b}_{2n+1}^\dagger \hat{a}_{2n} + \hat{b}_{2n-1}^\dagger \hat{a}_{2n} + \text{h.c.} \right] + \sum_n \left[(\Phi_n + M) \hat{a}_{2n}^\dagger \hat{a}_{2n} + (\Phi_n - M) \hat{b}_{2n+1}^\dagger \hat{b}_{2n+1} \right]. \quad (8)$$

Identifying $\hat{c}_{2n} = \hat{a}_{2n}$ and $\hat{c}_{2n+1} = \hat{b}_{2n+1}$, this takes the form of the well known Fermi-Hubbard Hamiltonian for a one-dimensional lattice

$$\hat{H} = -J \sum_n \left[\hat{c}_{n+1}^\dagger \hat{c}_n + \hat{c}_n^\dagger \hat{c}_{n+1} \right] + \sum_n V_n \hat{c}_n^\dagger \hat{c}_n, \quad (9)$$

with hopping rate J and on-site potentials V_n . This Hamiltonian will be the starting point for the design of the optical lattice analogy. But before we proceed, we note that the free part \hat{H}_0 of this Hamiltonian, i.e., with $\Phi_n = 0$, can be explicitly diagonalized. Performing a discrete Fourier transform on the lattice

$$\hat{a}_p := \sum_n e^{-2inap} \hat{a}_{2n}, \quad \hat{b}_p := \sum_n e^{-i(2n+1)ap} \hat{b}_{2n+1}, \quad (10)$$

for $p \in (-\pi/2a, \pi/2a)$ and introducing new operators

$$\begin{aligned} \begin{pmatrix} \hat{A}_p \\ \hat{B}_p \end{pmatrix} &= \frac{1}{\sqrt{2E_p}} \begin{pmatrix} \sqrt{E_p + M} & \sqrt{E_p - M} \\ -\sqrt{E_p - M} & \sqrt{E_p + M} \end{pmatrix} \cdot \begin{pmatrix} \hat{a}_p \\ \hat{b}_p \end{pmatrix} \\ &= U_p \cdot \begin{pmatrix} \hat{a}_p \\ \hat{b}_p \end{pmatrix} \end{aligned} \quad (11)$$

we obtain the diagonalized form

$$\hat{H}_0 = \int dp E_p \left[\hat{A}_p^\dagger \hat{A}_p - \hat{B}_p^\dagger \hat{B}_p \right] \quad (12)$$

with the energy spectrum

$$E_p = \sqrt{M^2 + \frac{1}{4a^2} \cos^2(ap)}. \quad (13)$$

It approximates the relativistic energy-momentum relation at the edge of the Brillouin zone, for $p \approx \pm\pi/(2a)$. The spectrum of \hat{H}_0 consists thus of two symmetric intervals separated by a gap of $2M$. In order to obtain a positive Hamiltonian, we perform the usual re-definition $\hat{B}_p^\dagger \leftrightarrow \hat{B}_p$ which corresponds to changing the vacuum state by filling all \hat{B}_p states by a fermion. This is completely analogous to the *Dirac sea* picture in quantum electrodynamics. In terms of this analogy, \hat{A}_p^\dagger or \hat{A}_p create or annihilate an electron whereas \hat{B}_p or \hat{B}_p^\dagger create or annihilate a hole in the *Dirac sea* – which is then a positron. An additional potential Φ_n , if sufficiently localized in space, will not modify this spectrum but may introduce isolated eigenvalues with eigenstates corresponding to bound states localized in space.

Experimental set-up The Fermi-Hubbard Hamiltonian (9) can be realized with ultra-cold fermionic atoms in a one-dimensional optical lattice with the potential

$$W(x) = W_0 \sin^2(2kx) + \Delta W \sin^2(kx), \quad (14)$$

where $k = \pi/(2a)$, by taking $W_0 \gg \Delta W$. Similar settings have already been obtained experimentally [22].

Although discretization of $W(x)$ at $x_n = na$ gives directly V_n of (9), the small perturbation ΔW doubles the original periodicity of the potential $W(x)$ and thus some mathematical caution in treating ΔW perturbatively is required. By a version of WKB approximation for periodic potentials [21], we re-derive the Hubbard model and the energy band structure from first principles, using two sets of Wannier functions localized in the “upper” and the “lower” minima of the potential $W(x)$, respectively. An interesting universal phenomenon occurs, see Fig. 1. For $\Delta W = 0$, the lowest band is de-

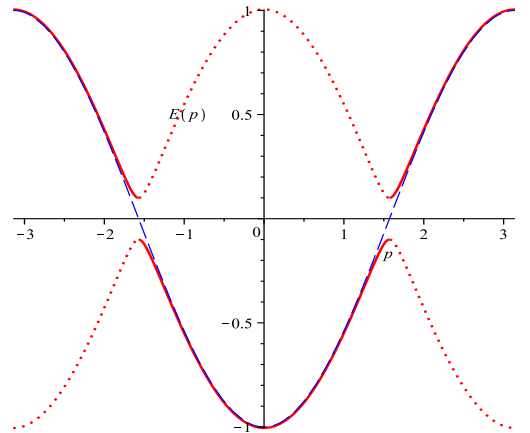


FIG. 1: Sketch of the dispersion relation (in units of J and $1/a$) for $\Delta W = 0$ (dashed blue curve) and small $\Delta W > 0$ (solid and dotted red curves).

scribed, in the *nearest-neighbor approximation* used here, by $E_p = -J \cos(ap)$ (the dashed blue curve in Fig. 1).

Switching on small $\Delta W > 0$, which immediately doubles the period of the potential, forces the energy dispersion relation to halve its period (the Brillouin zone shrinks by factor 2) while keeping similar functional dependence on p when $\Delta W \ll W_0$. It leads to splitting of this band into two sub-bands (red solid and dotted curves in Fig. 1) which are approximately described by

$$E_{\pm}(p) = \pm \sqrt{M^2 + J^2 \cos^2(ap)}. \quad (15)$$

This approximation reproduces the relativistic relation (13) for $J = 1/(2a)$ and holds uniformly for all values of the quasi-momentum p when $J^2 \sim T$ and $M \sim \Delta W$ are small and T is the transmission probability through the potential barrier [25]. In the vicinity of the minimum of the upper band and the maximum of the lower band, separated by a gap $2M$, it reproduces the relativistic energy-momentum relation. The corresponding Hamiltonian has the same form as the one for the discretized Dirac equation (12), thus completing the analogy.

Using again the WKB approximation, we find that the hopping rate J is mainly determined by the potential strength W_0 , the laser wave-number k and the mass m_{atom} of the atoms (not to be confused with the effective mass M of the Dirac particles to be simulated)

$$J \approx \frac{4}{\pi} \sqrt{W_0 E_R} \exp \left\{ -\frac{\pi}{4} \sqrt{\frac{W_0}{E_R}} \right\}, \quad (16)$$

where $E_R = k^2/2m_{\text{atom}} = \pi^2/(8m_{\text{atom}}a^2)$ is the recoil energy. The correction ΔW generates the mass gap $M \approx \Delta W/2$. The analogue of the e^+e^- pair creation can be simulated if the involved scales obey the hierarchy

$$\omega_{\text{osc}} \gg J \gg M \gg T. \quad (17)$$

First, the local oscillator frequency ω_{osc} in the potential minima must be smaller than J to ensure the applicability of the single-band Fermi-Hubbard Hamiltonian (9). Second, $J \gg M$ is required for the continuum limit, i.e., that the discretized expression (5) provides a good approximation. Similarly, the change $\Delta\Phi_n = \Phi_{n+1} - \Phi_n$ of the analogue of the electrostatic potential Φ_n from one site to the next should be smaller than M . Over many sites, however, this change can well exceed the mass gap $2M$, which is basically one of the conditions for the Schwinger effect to occur. Finally, the effective temperature T should be well below the mass gap $2M$ in order to avoid thermal excitations.

Let us insert some example parameters. For ${}^6\text{Li}$ atoms in an optical lattice made of light with a wavelength of 500 nm, the recoil energy E_R would be around $7 \mu\text{K}$. If we choose the potential strength as $W_0 = 10 \mu\text{K}$, the hopping rate J would be around $5 \mu\text{K}$ which is still sufficiently below the local oscillator frequency ω_{osc} of around $34 \mu\text{K}$. With $\Delta W = 1 \mu\text{K}$ we would get a mass M of 500 nK and the effective temperature should be below that value.

Bose-Fermi mapping Since it is typically easier to cool down bosonic than fermionic atoms, let us discuss an alternative realization based on bosons in an optical lattice. To this end, we start with the Bose-Hubbard Hamiltonian which has the same form as the Fermi-Hubbard Hamiltonian (8) after replacing the fermionic \hat{c}_n by bosonic \hat{d}_n operators, but with an additional on-site repulsion term $U(\hat{d}_n^\dagger \hat{d}_n - 1)\hat{d}_n^\dagger \hat{d}_n$. For large $U \gg J$ (which can be controlled by an external magnetic field via a Feshbach resonance, for example), we obtain the bosonic analogue of ‘‘Pauli blocking’’, i.e., at most one particle can occupy each site. Neglecting all states with double or higher occupancy, we can map these bosons exactly onto fermions in one spatial dimension via

$$\hat{d}_n = \exp \left(-i\pi \sum_{m < n} \hat{c}_m^\dagger \hat{c}_m \right) \hat{c}_n. \quad (18)$$

As a result, we obtain the same physics as described by the Fermi-Hubbard Hamiltonian (8).

Simulation of the Schwinger effect The above established analogy between the (discretized) quantum many-particle Hamiltonian of electrons and positrons in an electric field, on the one hand, and the (Bose or Fermi) Hubbard model describing ultra-cold atoms in optical lattices, on the other hand, enables laboratory simulations of relativistic phenomena of strong-field QED. Probably the most prominent of them is the spontaneous pair creation in strong electric fields known also as the Schwinger effect [1–3] which has to date not been confirmed experimentally. The original Schwinger effect [1] deals with a constant electric field E and would correspond to a static tilted optical lattice with $\Phi(x) = Ex$. However, an electric field which is localized in space and time is of course more realistic. In order to clearly distinguish the non-perturbative Schwinger effect (via tunneling) from other perturbative effects such as dynamical pair creation, the electric field should be slowly varying (compared to the scale of the gap $2M$).

As a result, we envisage an experimental realization sketched in Fig. 2. In order to prepare the initial state, we start with $\Delta W \gg W_0$ where the two bands are separated by a large gap. The *Dirac sea* then corresponds to the state where all lower minima are filled with atoms while all upper minima are empty (half filling of the lattice, see first picture in Fig. 2). If we then decrease ΔW adiabatically until $\Delta W \ll W_0$ and thus $J \gg M$, the atoms become delocalized – but still the lower band is filled while the upper band remains empty (second picture in Fig. 2). As the next stage, we slowly deform the lattice in order to mimic an electric field Φ and to facilitate tunneling from the lower band to the upper band – which is the analogue of the Schwinger effect (third picture in Fig. 2). Finally, after slowly straightening out the lattice again (fourth picture in Fig. 2), we increase ΔW adiabatically until $\Delta W \gg W_0$. By this energetic

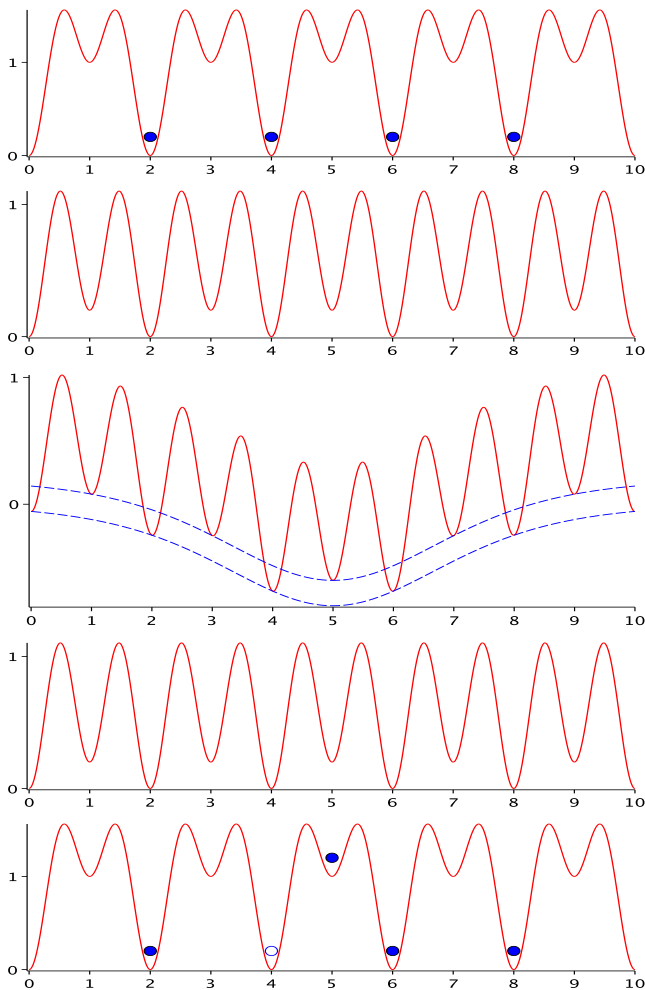


FIG. 2: Sketch (not to scale) of the stages of the simulation (from top to bottom). The solid red curves represent the optical lattice potentials $W(x)$ as a function of position x and the dashed blue curves correspond to the effective electric potential Φ . The blue solid dots are particles and the empty circle is a hole.

separation, a particle-hole pair created via the analogue of the Schwinger effect is then being transformed to an atom in one of the upper minima and, consequently, a missing atom in one of the lower minima (fifth picture in Fig. 2). This could be detected by site-resolved imaging [20], for example.

Apart from investigating the pair creation probability for space-time dependent electric fields $E(t, x)$, this quantum simulator for the Schwinger effect could provide some insight into the impact of interactions. For example, including dipolar interactions of the atoms, we may even switch between attractive and repulsive interactions by aligning the atoms spins parallel or perpendicular to the lattice. Note that this goes far beyond the simula-

tion of the classical Dirac equation and requires the full quantum many-particle Hamiltonian.

* e-mail:nikodem.szpak@uni-due.de

† e-mail:ralf.schuetzhold@uni-due.de

- [1] J. Schwinger, Phys. Rev. **82**, 664 (1951).
- [2] F. Sauter, Z. Phys. **69**, 742 (1931); *ibid.* **73**, 547 (1931).
- [3] W. Heisenberg and H. Euler, Z. Phys. **98**, 714 (1936). V. Weisskopf, Kong. Dans. Vid. Selsk., Mat.-fys. Medd. **XIV**, 6 (1936).
- [4] G. V. Dunne, H. Gies, R. Schützhold, Phys. Rev. **D80**, 111301 (2009).
- [5] R. Schützhold, H. Gies, G. Dunne, Phys. Rev. Lett. **101**, 130404 (2008).
- [6] C. K. Dumlu, G. V. Dunne, Phys. Rev. Lett. **104**, 250402 (2010).
- [7] See, e.g., the European ELI programme: <http://www.extreme-light-infrastructure.eu/>
- [8] P. A. M. Dirac Proc. Roy. Soc. (London) A **117**, 610 (1928); *ibid.* **118**, 351 (1928); *ibid.* **126**, 360 (1930).
- [9] R. Gerritsma, B. P. Lanyon, G. Kirchmair, F. Zähringer, C. Hempel, J. Casanova, J. J. García-Ripoll, E. Solano, R. Blatt, and C. F. Roos, Phys. Rev. Lett. **106**, 060503 (2011).
- [10] S.-L. Zhu, B. Wang, and L.-M. Duan, Phys. Rev. Lett. **98**, 260402 (2007).
- [11] J.-M. Hou, W.-X. Yang, and X.-J. Liu, Phys. Rev. A **79**, 043621 (2009).
- [12] L.-K. Lim, C. M. Smith, and A. Hemmerich, Phys. Rev. Lett. **100**, 130402 (2008).
- [13] O. Boada, A. Celi, J. I. Latorre, and M. Lewenstein, ArXiv e-prints (2010), 1010.1716.
- [14] W. G. Unruh and R. Schützhold, Phys. Rev. D **68**, 024008 (2003).
- [15] N. Goldman, A. Kubasiak, A. Bermudez, P. Gaspard, M. Lewenstein, and M. A. Martin-Delgado, Phys. Rev. Lett. **103**, 035301 (2009).
- [16] R. Gerritsma, G. Kirchmair, F. Zähringer, E. Solano, R. Blatt, and C. F. Roos, Nature **463**, 68 (2010).
- [17] L. Lamata, J. León, T. Schätz, and E. Solano, Phys. Rev. Lett. **98**, 253005 (2007).
- [18] K. S. Novoselov, A. K. Geim, S. V. Morozov, D. Jiang, M. I. Katsnelson, I. V. Grigorieva, S. V. Dubonos, and A. A. Firsov, Nature **438**, 197 (2005).
- [19] M. I. Katsnelson, K. S. Novoselov, and A. K. Geim, Nature Physics **2**, 620 (2006).
- [20] J. F. Sherson, C. Weitenberg, M. Endres, M. Cheneau, I. Bloch, and S. Kuhr, Nature **467**, 68 (2010).
- [21] N. L. Balazs, Annals of Physics **53**, 421 (1969).
- [22] T. Salger, G. C., K. S., and W. M., Phys. Rev. Lett. **99**, 190405 (2007).
- [23] F. Finkel, A. Goñalez-Lopez, and M. A. Rodriguez, J. Phys. A: Math. Gen. **32**, 6821 (1999).
- [24] A. D. Hemery and A. P. Veselov, J. Math. Phys. **51**, 072108 (2010).
- [25] Details of this theory will be published elsewhere.